Hindawi
Complexity
Volume 2019, Article ID 7973823, 11 pages
https://doi.org/10.1155/2019/7973823

Research Article

Time-Delayed Feedback Control in the Multiple Attractors Wind-Induced Vibration Energy Harvesting System

Qin Guo, Zhongkui Sun, Ying Zhang, and Wei Xu

Department of Applied Mathematics, Northwestern Polytechnical University, Xi'an 710072, Shaanxi, China

Correspondence should be addressed to Wei Xu; weixu@nwpu.edu.cn

Received 7 September 2018; Revised 14 November 2018; Accepted 9 December 2018; Published 1 January 2019

Academic Editor: Giacomo Innocenti

This paper proposes a time-delayed feedback control to improve collection performance of the multiple attractors wind-induced vibration energy harvester system. By employing a conversion mechanism for decoupling the electromechanical equations and the stochastic averaging method, the roles of the time-delayed feedback and the system parameters have been systematically examined. In the deterministic case, the time delay can control efficiently the birhythmic properties; thus one can realize a dividing line in the parameter plane that separates the space into two subspaces of generically distinct nature. Further, it is exclusively demonstrated that implementing time-delayed feedback control serves as a very simple but highly efficient scheme to increase the harvested energy from vibrations in presence of noise disturbances. Additionally, the time constant ratio and coupling coefficients can also be properly tuned to optimize power generation.

1. Introduction

Growing demand of electrical energy and environmental issues has spurred considerable efforts to generate electricity from renewable energy sources [1]. Energy harvesting systems which served as a promising solution for generating electricity are designed to transform available ambient energy (e.g., wind energy, solar energy, tidal energy, piezoelectricity, thermoelectricity, and kinematic energy) into electrical energy for small and/or portable devices [2]. Although common transduction mechanisms are electromagnetic, piezoelectric, and electrostatic, the piezoelectric conversion mechanism is in general preferable due to its good power generation performance, simple structure, and no reliance on external magnetic field or initial DC voltage [3].

In the early stages, different types of linear vibration energy harvesters have been designed to generate electrical energy [4–6]. These systems, however, were found to be effective within a limited bandwidth near their resonant frequencies, thus limiting their application to frequency variant, amplitude variant, broadband, and random excitation sources which are typical excitation types in real applications [2, 7, 8]. In order to solve this critical challenge, a burst of research activities have been devoted to widen the working frequency of energy harvesters by using nonlinear phenomenon [9–14].

Compared to linear systems, nonlinear systems can generate electrical energy over a larger continuous bandwidth and are less sensitive to changes in frequency characteristics [14]. Nonlinear monostable, bistable, and tristable energy harvesters have been successively explored [13, 15, 16]. Sebald [13] experimentally proved that the operating bandwidth of the nonlinear monostable energy collector is several times that of its linear counterpart. One of the drawbacks of monostable design is its poor performance when the excitation is random excitation [17, 18]. Therefore, research interests have turned to collectors that utilize multiple steady states. The unique advantage of bistable energy harvesters (BEH) has been demonstrated by Cottone et al. [19] from the viewpoint of stochastic resonance. Daqaq et al. [20] compared the energy harvesting performance between the BEH and monostable energy harvesters influenced by Gaussian white noise. Utilization of high-energy orbits in the bistable structural configuration for electrostatic, electromagnetic, and magnetostrictive transduction mechanisms is summarized by Erturk et al. [21]. More recently, Li et al. [22] demonstrated the better energy harvesting performance of the tristable

energy harvester (THE) over its bistable counterpart under random base excitations. A tristable energy harvesting system with fractional-order viscoelastic material has been meticulously elaborated in [23]. Further work in nonlinearity can include internal resonance, coherence resonance[12, 24], and parametric excitation [25–29].

From the perspective of vibration suppression, the reduced amplitude of the vibration is beneficial. For energy harvesting systems, however, amplitude reduction is undesirable because the resultant energy is reduced. Consequently, more advanced control methods (e.g. synchronized switching harvesting on inductor and switching controller) have been proposed to solve this critical problem [30, 31]. A simple and effective control strategy is time-delayed feedback control, which has been widely used to control bifurcation, chaos, resonance, and birhythmicity [32–36]. In addition, as an important renewable energy source, wind energy has received extensive attention from scholars [2, 31]. In this paper, we will focus on the multiple attractors wind-induced vibration energy harvesting system [2] and unveil the optimization effect of time-delayed feedback control on this system with random excitation.

The rest of this paper is organized as follows. The next section makes a detailed description of multiple attractors energy harvesting system with time-delayed feedback control and Gaussian white noise excitation and carries on a detailed theoretical analysis. The main deterministic and random theoretical and numerical contributions are presented in Sections 3 and 4, respectively. Finally, the results are concluded and summarized in Section 5.

2. Model and Its Analytical Estimates

2.1. Nonlinear Vibration Energy Harvesting System with Delayed Feedback. A schematic of a multiple attractors wind-induced vibration energy harvester system at low Reynolds number is shown in Figure 1 (see [2]). The physical model consists of a flexible beam with distributed piezoelectric patches and an electrical circuit having a load resistance R_l. The dimensionless form of the original model is dominated by the following set of equations [2, 37]:

$$\ddot{x} + \mu\left(-\dot{x} + \frac{1}{3}(\dot{x})^3 - \frac{\alpha}{5}(\dot{x})^5 + \frac{\beta}{7}(\dot{x})^7\right) + w_0^2 x = \eta_0 v,$$
$$\dot{v} + \gamma v = -\eta_1 \dot{x}. \tag{1}$$

Here x is the dimensionless transversal beam deflection function and the coefficients μ, α, β are related to wind velocity, fluid mass density, Reynolds number, etc. v is the dimensionless form of the voltage across an equivalent resistive load R_l and γ is time constant ratio ($\gamma = 1/R_l C_p$, C_p is inherent capacitance of the piezoelectric element). η_0 is the piezoelectric coupling coefficient in the mechanical equation and η_1 is the piezoelectric coupling coefficient in the electrical equation. A time-delayed feedback is known as an efficient tool [35, 36] for continuous-time control of dynamical systems [38]. A simple and efficient scheme of time-delayed feedback control is Pyragas control since it does not require detailed information of the system to be controlled [38]. Of particular interest to us is such a form of feedback $F(t) = k[\dot{x}(t-\tau) - \dot{x}(t)]$, where $\dot{x}(t)$ is the signal coming from the system, k is the feedback strength, and τ is the time delay. This control method by changing both the feedback strength and time delay has also been applied in a multicycle van der Pol oscillator [35].

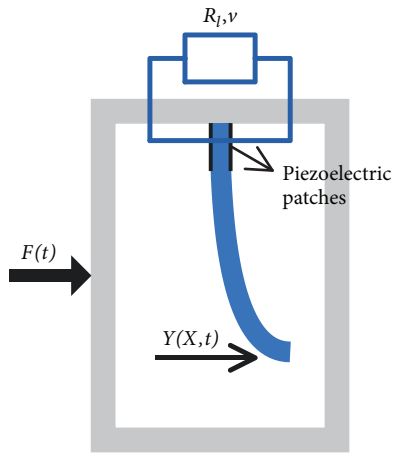

Figure 1: Schematic representation of the energy harvesting system under wind flow excitation with low Reynolds number.

The object of this paper is to understand the dynamic responses of the energy harvester system toward such a delayed feedback control. On the other hand, the energy harvesting system is inevitably affected by random excitation. This paper introduces Gaussian white noise as a random noise source. Application of delayed feedback and consideration of Gaussian white noise excitation result in the following equation:

$$\ddot{x} + \mu\left(-\dot{x} + \frac{1}{3}(\dot{x})^3 - \frac{\alpha}{5}(\dot{x})^5 + \frac{\beta}{7}(\dot{x})^7\right) + w_0^2 x = \eta_0 v + k(\dot{x}_\tau - \dot{x}) + \xi(t), \tag{2}$$

$$\dot{v} + \gamma v = -\eta_1 \dot{x}. \tag{3}$$

Here $\xi(t)$ is Gaussian white noise which has the following properties $\langle \xi(t) \rangle = 0$, $\langle \xi(t)\xi(t+\tau) \rangle = 2D\delta(\tau)$. $\dot{x}_\tau$ stands for the delayed variable $\dot{x}(t-\tau)$, k is the strength of the delayed feedback. And τ defines the time delay ($\tau > 0$) characterizing the finite time in signal propagation, in measuring and estimating the system states, calculating and executing the control force, etc.

2.2. Analytic Estimates of Nonlinear Vibration Energy Harvesting System. Suppose that (2) has the following form of solution:

$$x = a(t)\cos\phi,$$
$$\dot{x} = -a(t)\, w_0 \sin\phi, \tag{4}$$

where $\varphi = w_0 t + \theta(t)$, $a(t)$ is the amplitude, and $\theta(t)$ is the phase angle. Then [39]

$$\begin{aligned}\dot{x}_\tau &= -aw_0 \sin\phi \cos\left(w_0\tau\right) + a\cos\phi w_0 \sin\left(w_0\tau\right)\\ &= \dot{x}\cos\left(w_0\tau\right) + xw_0 \sin\left(w_0\tau\right).\end{aligned} \tag{5}$$

Further, substituting Eq. (4) into Eq. (3) yields [40]

$$v\left(t\right) = C\left(t\right)e^{-\lambda t} - \frac{a\eta_1 w_0}{\gamma^2 + {w_0}^2}\left(w_0\cos\varphi - \gamma\sin\varphi\right). \tag{6}$$

The steady part of (6) is

$$\begin{aligned}v\left(t\right) &= -\frac{a\eta_1 w_0}{\gamma^2 + {w_0}^2}\left(w_0\cos\varphi - \gamma\sin\varphi\right)\\ &= -\frac{\eta_1 {w_0}^2}{\gamma^2 + {w_0}^2}x - \frac{\eta_1\gamma}{\gamma^2 + {w_0}^2}\dot{x}.\end{aligned} \tag{7}$$

Due to

$$w_0\cos\phi - \gamma\sin\phi = \sqrt{\gamma^2 + {w_0}^2}\cos\left(\phi + \tan^{-1}\frac{\gamma}{w_0}\right), \tag{8}$$

the amplitude of the steady-state voltage is

$$B = \frac{a\eta_1 w_0}{\sqrt{\gamma^2 + {w_0}^2}}. \tag{9}$$

Substitution of (5) and (7) into (2) yields a modified governing equation for a nonlinear energy harvester

$$\begin{aligned}&\ddot{x} + w_0^2 x + \mu\left(-\dot{x} + \frac{1}{3}\dot{x}^3 - \frac{\alpha}{5}\dot{x}^5 + \frac{\beta}{7}\dot{x}^7\right) + \frac{\eta_0\eta_1 {w_0}^2}{\gamma^2 + {w_0}^2}x\\ &\quad + \frac{\eta_0\eta_1\gamma}{\gamma^2 + {w_0}^2}\dot{x}\\ &\quad = k\left(\dot{x}\cos\left(w_0\tau\right) + xw_0\sin\left(w_0\tau\right) - \dot{x}\right) + \xi\left(t\right).\end{aligned} \tag{10}$$

To facilitate the analysis, we use the following substitutions:

$$\begin{aligned}S &= 1 - \frac{\eta_0\eta_1\gamma}{\mu\left(\gamma^2 + w_0^2\right)} - \frac{k}{\mu}\left(1 - \cos\left(w_0\tau\right)\right),\\ w^2 &= w_0^2 + \frac{\eta_0\eta_1 w_0^2}{\gamma^2 + w_0^2} - kw_0\sin\left(w_0\tau\right).\end{aligned} \tag{11}$$

The new form of the equations is thus

$$\ddot{x} + \mu\left(-S\dot{x} + \frac{1}{3}\dot{x}^3 - \frac{\alpha}{5}\dot{x}^5 + \frac{\beta}{7}\dot{x}^7\right) + w^2 x = \xi\left(t\right). \tag{12}$$

On the hypothesis that damping and noise intensity D is small, introduce a transformation of variables [41]

$$\begin{aligned}x\left(t\right) &= a\left(t\right)\cos\phi,\\ \dot{x}\left(t\right) &= -a\left(t\right)w\sin\phi,\\ \phi &= wt + \theta.\end{aligned} \tag{13}$$

By applying (13) into (12), the differential functions versus $a(t), \theta(t)$ can be obtained

$$\begin{aligned}\dot{a} = \frac{\sin\phi}{w}&\left\{\mu\left[S\left(-aw\sin\phi\right) - \frac{1}{3}\left(-aw\sin\phi\right)^3\right.\right.\\ &\left. + \frac{\alpha}{5}\left(-aw\sin\phi\right)^5 - \frac{\beta}{7}\left(-aw\sin\phi\right)^7\right] + w^2 a\cos\phi\\ &\left. - \xi\left(t\right)\right\},\\ \dot{\theta} = \frac{\cos\phi}{aw}&\left\{\mu\left[S\left(-aw\sin\phi\right) - \frac{1}{3}\left(-aw\sin\phi\right)^3\right.\right.\\ &\left. + \frac{\alpha}{5}\left(-aw\sin\phi\right)^5 - \frac{\beta}{7}\left(-aw\sin\phi\right)^7\right] + w^2 a\cos\phi\\ &\left. - \xi\left(t\right)\right\},\end{aligned} \tag{14}$$

By adopting the standard stochastic averaging method [41], the stochastic differential equations (in the Itŏ sense) for the instantaneous amplitude $a(t)$ and phase $\theta(t)$ are determined by

$$\begin{aligned}da &= \left[-\frac{\mu}{128w}\left(5\beta\left(aw\right)^7 - 8\alpha\left(aw\right)^5 + 16\left(aw\right)^3\right.\right.\\ &\quad \left.\left. - 64S\left(aw\right)\right) + \frac{D}{2aw^2}\right]dt + \frac{\sqrt{D}}{w}dW_1\left(t\right),\\ d\theta &= \frac{\sqrt{D}}{aw}dW_2\left(t\right).\end{aligned} \tag{15}$$

Thereby, $W_1(t)$ and $W_2(t)$ are independent normalized Wiener processes and S, w is given by (11). Obviously, the amplitude a does not depend on the phase θ. Consequently, the Fokker–Planck–Kolmogorov (FPK) equation of amplitude yields

$$\begin{aligned}\frac{\partial p\left(a,t\right)}{\partial t} &= -\frac{\partial}{\partial a}\left[A\left(a\right)p\left(a,t\right)\right]\\ &\quad + \frac{1}{2}\frac{\partial^2}{\partial a^2}\left[B\left(a\right)p\left(a,t\right)\right],\end{aligned} \tag{16}$$

with

$$\begin{aligned}A\left(a\right) &= -\frac{\mu}{128w}\left(5\beta\left(aw\right)^7 - 8\alpha\left(aw\right)^5 + 16\left(aw\right)^3\right.\\ &\quad \left. - 64S\left(aw\right)\right) + \frac{D}{2aw^2},\\ B\left(a\right) &= \frac{D}{w^2}.\end{aligned} \tag{17}$$

Considering the stationary case, the stationary probability density function (PDF) for amplitude can be solved as

$$\begin{aligned}P\left(a\right) = Na\exp&\left(-\frac{\mu}{64D}\left(\frac{5\beta}{8}\left(aw\right)^8 - \frac{4\alpha}{3}\left(aw\right)^6\right.\right.\\ &\left.\left. + 4\left(aw\right)^4 - 32S\left(aw\right)^2\right)\right),\end{aligned} \tag{18}$$

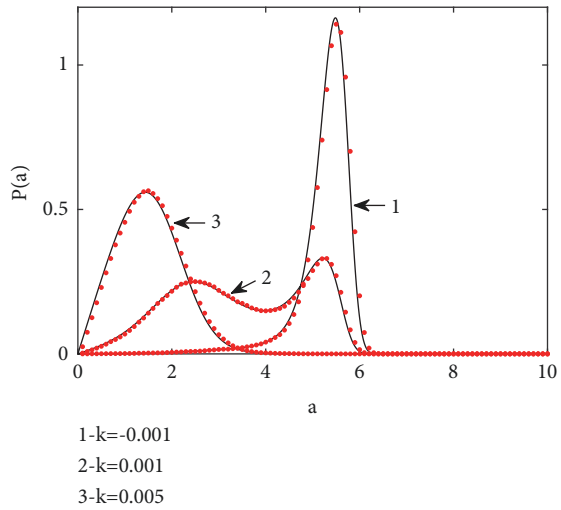

Figure 2: Stationary PDFs of the amplitude P (a) for various values of feedback strength k. The solid lines stand for the analytic results and the dots denote the numerical simulations of original system.

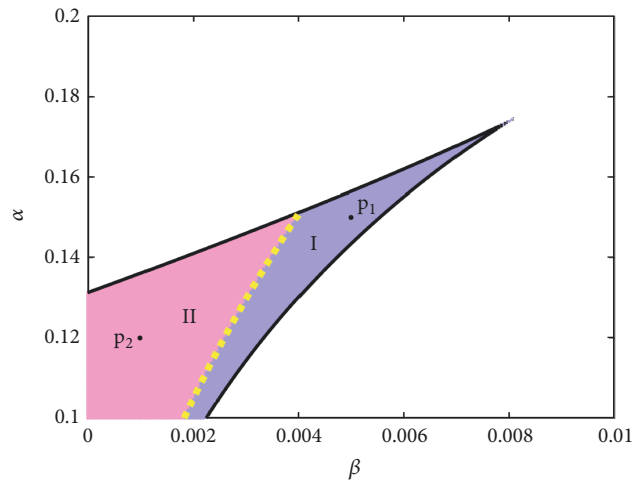

Figure 3: Parameter domain (α, β) for the existence of the three limit cycles (area denoted by the colored area without the dotted line in absence of delayed feedback) and a single limit cycle (area denoted by white region). The yellow dotted line denotes the bifurcation line characterizing the two parameter zones corresponding to the points $p_1(0.005, 0.15)$ and $p_2(0.001, 0.12)$ for two distinct dynamical scenarios in presence of delayed feedback corresponding to Figures 4(a) and 4(b), respectively.

in which N is a normalization constant and S, w is given by (11). Thus, the expected value of the mean square voltage can be calculated as

$$\left\langle v^2(t)\right\rangle = \left\langle B^2\right\rangle = \frac{\eta_1^2 w_0^2}{\gamma^2 + w_0^2}\left\langle a^2\right\rangle = \frac{\eta_1^2 w_0^2}{\gamma^2 + w_0^2}\int_0^{+\infty} a^2 P(a)\, da. \tag{19}$$

In this paper, the fixed parameters are $w_0 = 1$, $\mu = 0.01$. In order to validate the effectiveness of the analytical results (see (18)), direct numerical simulations based on the second-order Runge–Kutta algorithm (provided in the appendix) of (2), (3) are performed.

Letting $\alpha = 0.15$, $\beta = 0.005$, $D = 0.01$, $\tau = \pi$, $\eta_0 = 0.01$, $\eta_1 = 0.25, \gamma = 0.2$, Figure 2 demonstrates the stationary PDFs of the amplitude for three different values of feedback strength, respectively. In Figure 2, the solid lines are the analytical results and the dots result from numerical simulations. The basic agreement between the analytical results and numerical simulations best confirm the effectiveness of the theoretical analyses.

Observations of Figure 2 also show that the negative time delay feedback control induces an increase in the probability of large amplitude motion of the energy harvesting system.

3. Control of Birhythmicity Using Delayed Feedback without Noise

Letting $\partial P(a)/\partial a = 0$, the extreme a_m of the distribution of (18) is given by the roots of the following equation:

$$\frac{5\beta\mu}{64}(a_m w)^8 - \frac{\alpha\mu}{8}(a_m w)^6 + \frac{\mu}{4}(a_m w)^4 - S\mu(a_m w)^2 - D = 0. \tag{20}$$

For $D = 0$, the amplitude equation is dominated by

$$\frac{5\beta}{64}(a_m w)^6 - \frac{\alpha}{8}(a_m w)^4 + \frac{1}{4}(a_m w)^2 - S = 0. \tag{21}$$

It should be noted that the theoretical method in our paper is more accurate than the theoretical method proposed by Debabrata Biswas and his collaborators [37]. For the same parameters as in Figure 3 in [37], one can obtain that the Hopf bifurcation of the control parameter is approximately 0.0953 by using the continuation package XPPAUT. The theoretical value of the Hopf bifurcation of the control parameter in [2] is $d_{HB} = \mu = 0.1$. However, the theoretical value of the Hopf bifurcation of the control parameter that we derived is $k = \mu - \eta_0\eta_1\gamma/(\gamma^2 + w^2) \approx 0.095192$.

Based on (11) and (21), Figure 3 illustrates the bifurcation diagram in the $\alpha - \beta$ parameter domain for $\eta_0 = 0.01, \eta_1 = 0.25, \gamma = 0.2$. In absence of delayed feedback, the birhythmic region possessing a bistability mode with coexistence of two stable limit cycles (LC) of the system consists of all colored regions without the dotted line. The birhythmic region, whereas, is split into two parameter zones corresponding to the points $p_1(0.005, 0.15)$ for $\beta = 0.005, \alpha = 0.15$ and $p_2(0.001, 0.12)$ for $\beta = 0.001, \alpha = 0.12$ charactering two distinct dynamical scenarios in presence of delayed feedback ($k = 0.01$), which are verified in Figures 4(a) and 4(b), respectively. Observing Figure 4(a), when the time delay increases gradually from zero, the system shows an interesting transition from three limit cycles (two are stable limit cycles and the other is unstable) to a stable limit cycle then to a stable fixed point and thence to oscillation recovery for $p_1(0.005, 0.15)$. Four exemplary illustrations for $\tau = 0.2, 1.16, 3, 6$ are shown in Figure 5. For $\tau = 0.02$, the system exhibits birhythmic behavior possessing two stable

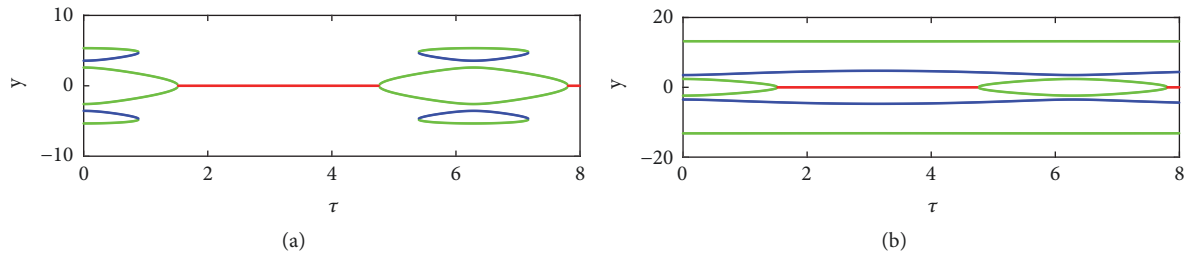

FIGURE 4: Bifurcation diagram of the energy harvesting system with τ for $k = 0.01$. (a) $\beta = 0.005, \alpha = 0.15$; (b) $\beta = 0.001, \alpha = 0.12$. The other parameters are $\eta_0 = 0.01, \eta_1 = 0.25, \gamma = 0.2$.

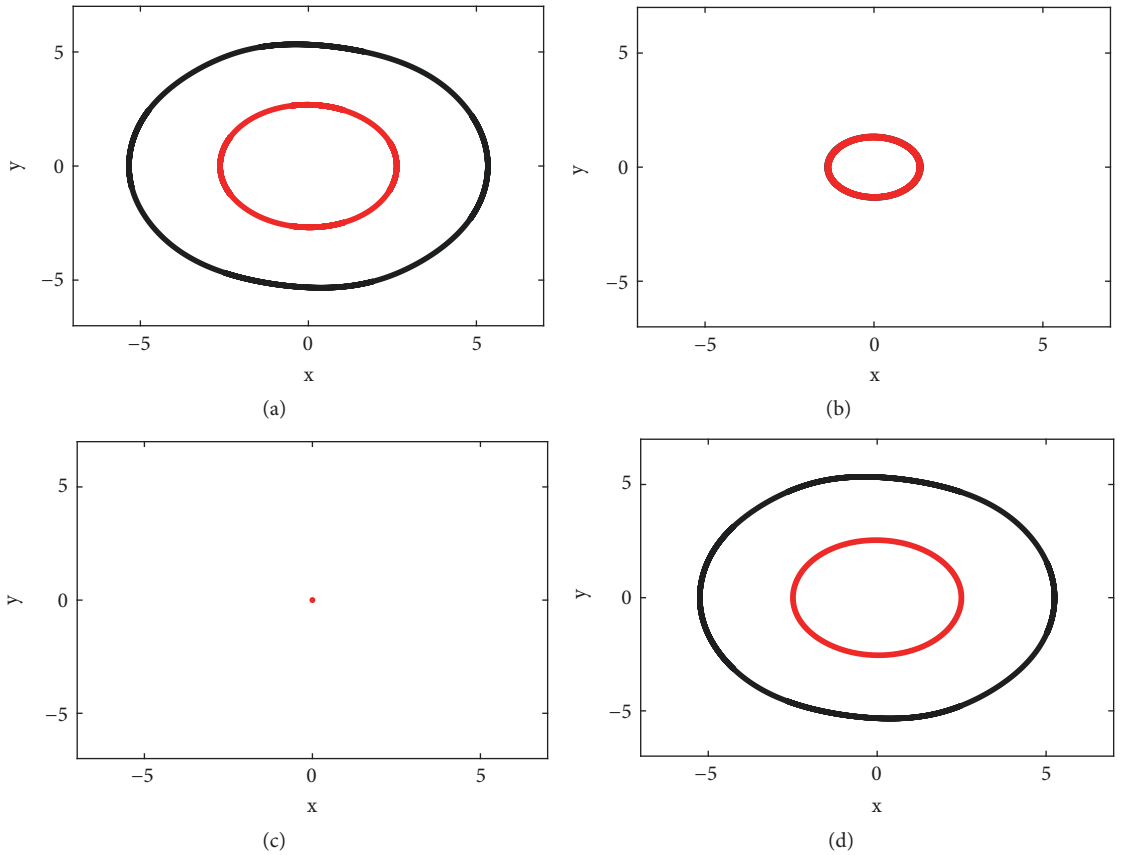

FIGURE 5: Phase plane plots corresponding to Figure 4(a). (a) $\tau = 0.2$, birhythmic oscillators; (b) $\tau = 1.16$, small-amplitude LC; (c) $\tau = 3.0$, stable steady state; (d) $\tau = 6.0$, birhythmic oscillators. The red line is for initial conditions $x = 0.1, \dot{x} = 0, v = 0.3$ and the black line is for the initial conditions $x = 7.0, \dot{x} = 0, v = 0.3$.

limit cycles as shown in Figure 5(a). With the gradual increase of time delay, the outer cycle ultimately vanishes beyond a critical time delay ($\tau > 1.5236$), and the system becomes monorhythmic in nature. This can be verified by Figure 5(b). As is shown in Figure 5(c), a further increase in time delay will cause the loss of self-sustained oscillatory character. Again with further increase of time delay, the system reproduces oscillation (Figure 5(d)).

Then, the evolution of the electric voltage of the harvested energy with time delay for $p1(0.005; 0.15)$ is exhibited in Figure 6. When the time delay increases slowly from zero, the system will have two different voltages due to the birhythmic nature of the system. For example, for initial condition $x = 0.1, \dot{x} = 0, v = 0.3$, the system's stable voltage is in the lower branch; for initial condition $x = 7.0, \dot{x} = 0, v = 0.3$, the system's stable voltage will be in the upper branch. As the time delay increases further, the system has only one stable voltage regardless of initial conditions. Again with further increase of time delay, the system will reside in a stable state with the voltage of 0. An further increase of the time delay will cause the system to resume oscillation, thereby generating electrical energy.

Comparing Figure 6 and the red curve of Figure 10, one can see that when the system is subjected to random

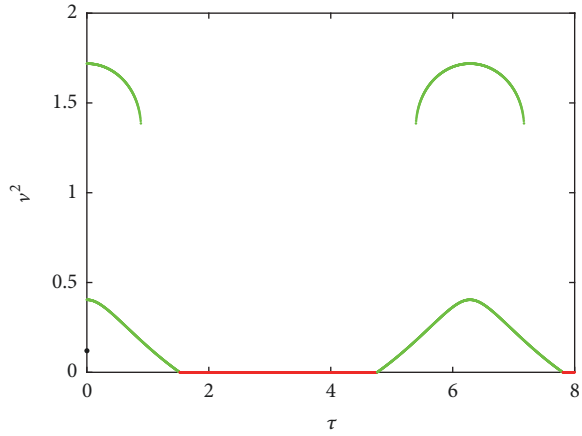

FIGURE 6: The dependence of the electric voltage v^2 on τ.

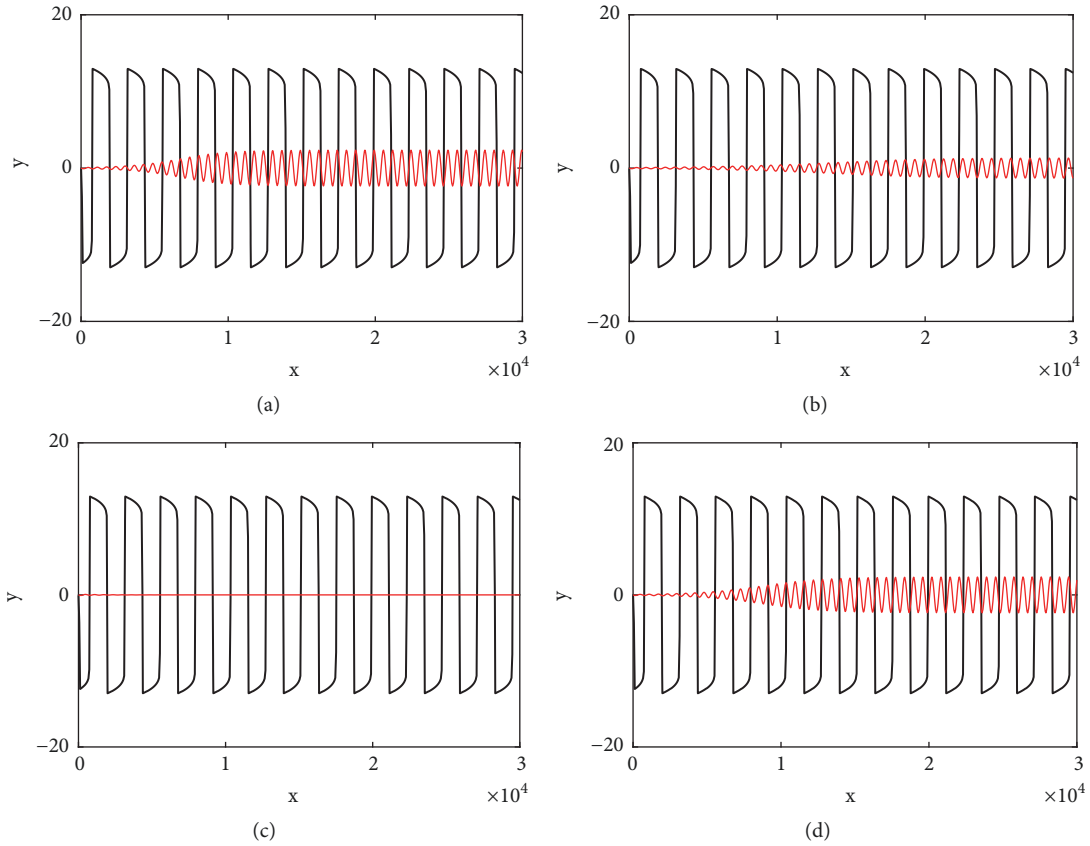

FIGURE 7: Time series corresponding to Figure 4(b). (a) $\tau = 0.2$, birhythmic oscillators; (b) $\tau = 1.16$, birhythmic oscillators; (c) $\tau = 3.0$, the bistable behaviors with coexistence of a stable LC and SSS; (d) $\tau = 6.0$, birhythmic oscillators. The red line is for initial conditions $x = 0.1, \dot{x} = 0, v = 0.3$ and the black line is for the initial conditions $x = 7.0, \dot{x} = 0, v = 0.3$.

perturbations, it will randomly jump between two limit cycle oscillations with different amplitudes without being affected by the initial conditions.

Further, we examine another dynamical scenario for $p_2(0.001, 0.12)$ as presented in Figure 4(b). For $\tau = 0.02$, the system exhibits birhythmic behavior possessing two stable limit cycles as shown in Figure 7(a). As the gradual increase of time delay, the inner cycle becomes smaller in amplitude and ultimately vanishes for a threshold of time delay about 1.5236, and the system exhibits the bistable behavior with coexistence of a stable LC and stable steady state (SSS). This can be verified by Figures 7(b) and 7(c), respectively. Again with further increase of time delay, the inner cycle reappears implying the recovery of birhythmicity (Figure 7(d)). By inspecting Figures 4(b) and 7, it can be also found that the time delay can hardly affect the outer stable cycle and the unstable limit cycle. The outer stable limit cycle that remains unaffected by time delay has an amplitude about 13.17.

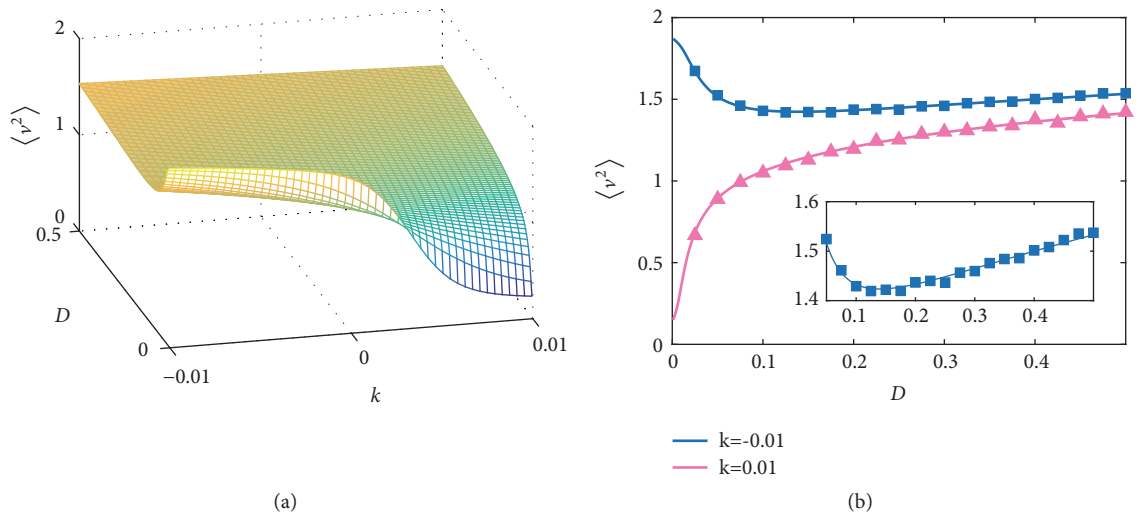

FIGURE 8: The dependence of the mean square electric voltage $\langle v^2 \rangle$ on D and k. Solid lines are the analytical results; symbols result from numerical simulations.

So based on the above findings, we can found that the delayed feedback can be suitably tuned to control the nature of the attractors depending on the parameter space. For the region II in Figure 3 where the point p_2 is located, the outer stable cycle is hardly affected by the time delay, which facilitates the energy harvester to be in a limit cycle of greater amplitude, thereby collecting more energy. So we will next focus on the region I and further explore the influence mechanism of time delay and noise on the points in the region to seek optimal control parameters.

4. Stochastic Responses

In the remaining part, we take the point $p_1(0.005, 0.15)$ for $\beta = 0.005, \alpha = 0.15$ in region I for further analysis. The effects of noise level, time delay and its feedback, time constant ratio, and coupling coefficients on mean square electric voltage will be explored in detail. In order to compare with the analytical results, direct numerical simulations of (2) and (3) are carried out, which verify the effectiveness of our theoretical predictions.

4.1. Effect of Noise Level. Figure 8 exhibits the dependence of the mean square electric voltage $\langle v^2 \rangle$ on the excitation intensity D and feedback strength k; the other parameters are $\eta_0 = 0.01, \eta_1 = 0.25, \gamma = 0.2, \tau = 1.0$. The solid lines stand for the analytic results and the symbols denote the numerical simulations of original system. For positive feedback, an increase in noise intensity causes the mean square voltage to increase sharply and then slowly increase. Surprisingly, for negative feedback strength, the mean square voltage will decrease rapidly as the noise level increases and then slowly increase (see a partial enlargement of Figure 8(b)). In general, the Gaussian white noise with high noise level helps to increase the collection capacity of the energy harvesting system, and the negative feedback strength is more favorable for the energy harvesting system to collect more energy than the positive feedback strength.

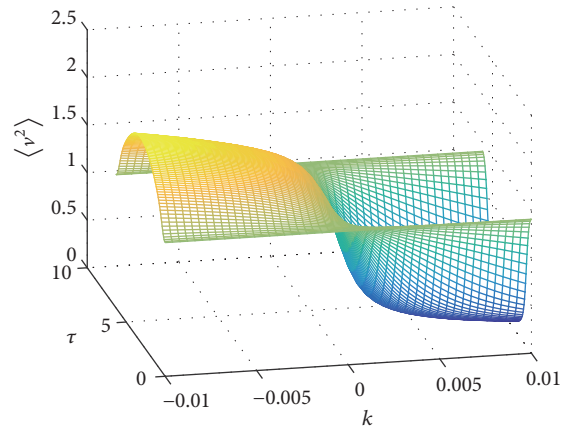

FIGURE 9: The dependence of the mean square electric voltage $\langle v^2 \rangle$ on τ and k.

4.2. Effect of Time Delay and Its Feedback. The dependence of the mean square electric voltage $\langle v^2 \rangle$ on the time delay τ and feedback strength k is depicted in Figure 9; the parameters are $\eta_0 = 0.01, \eta_1 = 0.25, \gamma = 0.2, D = 0.01$. This figure illustrates that the feedback strength makes the mean square voltage monotonously reduced, but the effect of time delay is nonmonotonic.

For an illustration of the impact of feedback strength on the mean square voltage, Figure 10(a) shows the change of the mean square voltage with feedback strength under two different time delay values $\tau = 1.0$ and $\tau = \pi$, which reveals that the mean square voltage decreases monotonically with the increase of the feedback strength and rapidly decays when the feedback strength increases to near zero.

Figure 10(b) further depicts the variation of the mean square voltage over time delay for $k = -0.01, 0.01$. As shown in Figure 10(b), the mean square voltage of the system without time-delayed feedback will stabilize at around 1.4. For $k = 0.01$, with time delay continuously grows, the mean square

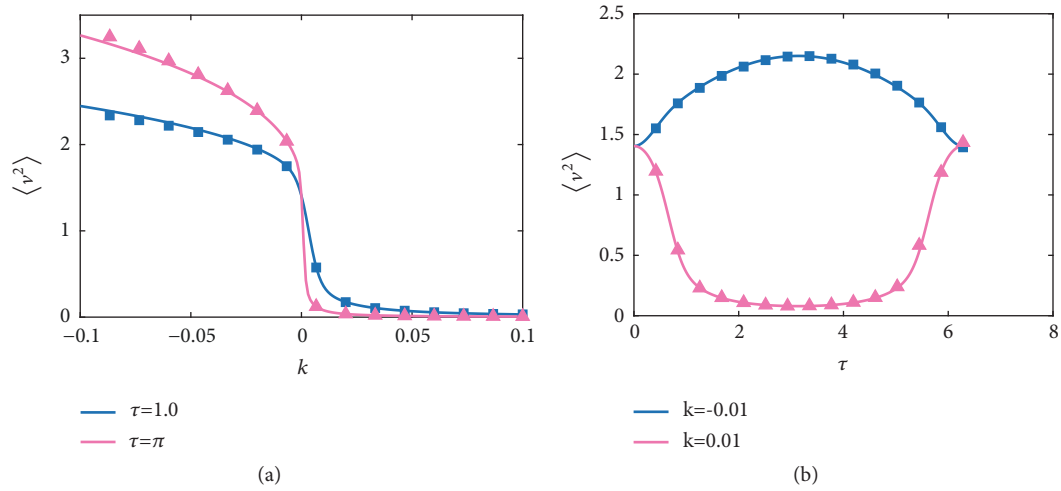

FIGURE 10: (a) The dependence of the mean square electric voltage $\langle v^2 \rangle$ on k. (b) The dependence of the mean square electric voltage $\langle v^2 \rangle$ on τ. Solid lines are the analytical results; symbols result from numerical simulations.

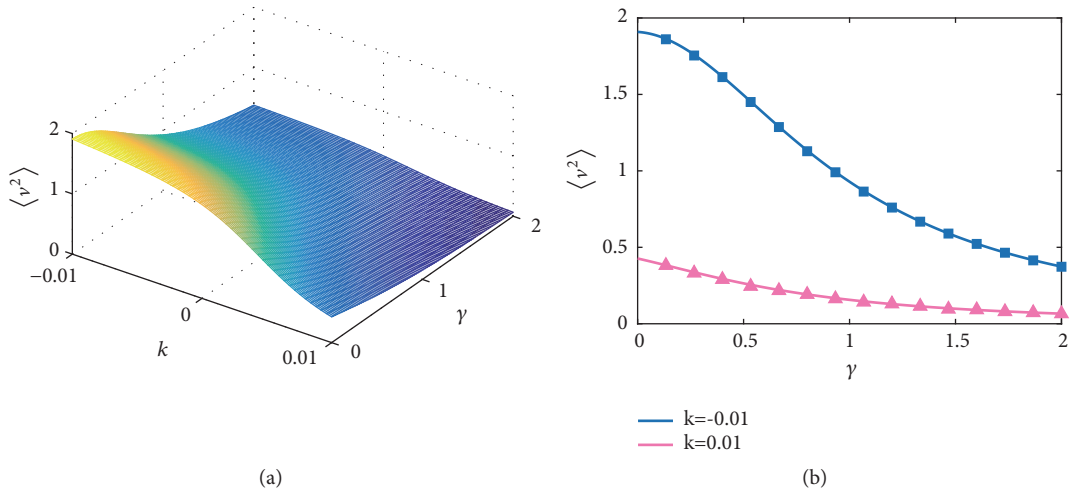

FIGURE 11: The dependence of the mean square electric voltage $\langle v^2 \rangle$ on k and γ. Solid lines are the analytical results; symbols result from numerical simulations.

voltage initially decreases monotonously, and it will show an upward trend after a gradual period. Surprisingly, with the monotonous increase of time delay, the mean square voltage initially monotonically increases, and it will undergo a monotonous decrease after exceeding the critical value $\tau = 3.141$ for $k = -0.01$. Based on the above analysis, one can get the optimal values of time delay and feedback strength are $k = -0.01, \tau = 3.141$ for this set of parameters, with which the system has the largest mean square voltage. Thus, the optimal control parameters k, τ can be selected to improve collection performance of the energy harvesting system.

4.3. Effect of Time Constant Ratio. The dependence of the mean square electric voltage $\langle v^2 \rangle$ on feedback strength k and time constant ratio γ is depicted in Figure 11; the parameters are $\eta_0 = 0.01, \eta_1 = 0.25, \tau = 1.0, D = 0.01$. For positive feedback strength, the mean square voltage decreases slowly with increasing time constant ratio (see the red curve in Figure 11(b)). However, for negative feedback strength, the mean square voltage decreases rapidly with increasing time constant ratio (see the blue curve in Figure 11(b)). And for a smaller time constant ratio, the mean square voltage at negative feedback strength is about 3-4 times the positive feedback strength. But for a larger time constant ratio, both the positive feedback strength and the negative feedback strength make the mean square voltage in a small range. That is, the negative feedback control and a smaller time constant ratio will induce larger mean square electric voltage.

4.4. Effect of Mechanical Coefficient. The dependence of the mean square electric voltage $\langle v^2 \rangle$ on η_0 and feedback strength k is depicted in Figure 12; the parameters are $\eta_1 = 0.25$, $\tau = 1.0, \gamma = 0.2, D = 0.01$. For smaller η_0, the mean square voltage will drop sharply under negative feedback strength $k = -0.01$ and will slowly decrease under positive feedback strength.

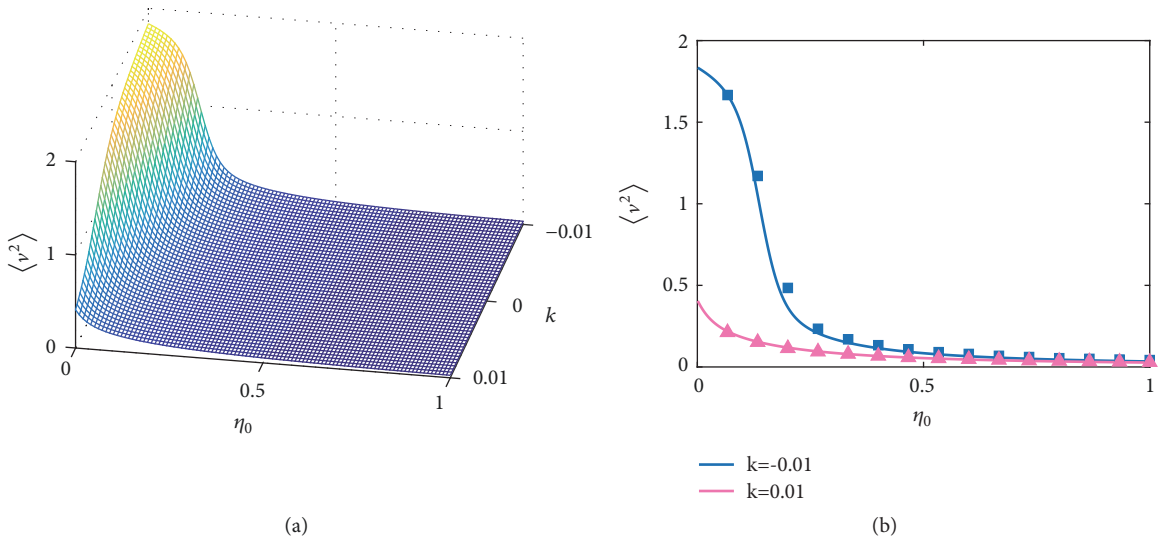

FIGURE 12: The dependence of the mean square electric voltage $\langle v^2 \rangle$ on k and η_0. Solid lines are the analytical results; symbols result from numerical simulations.

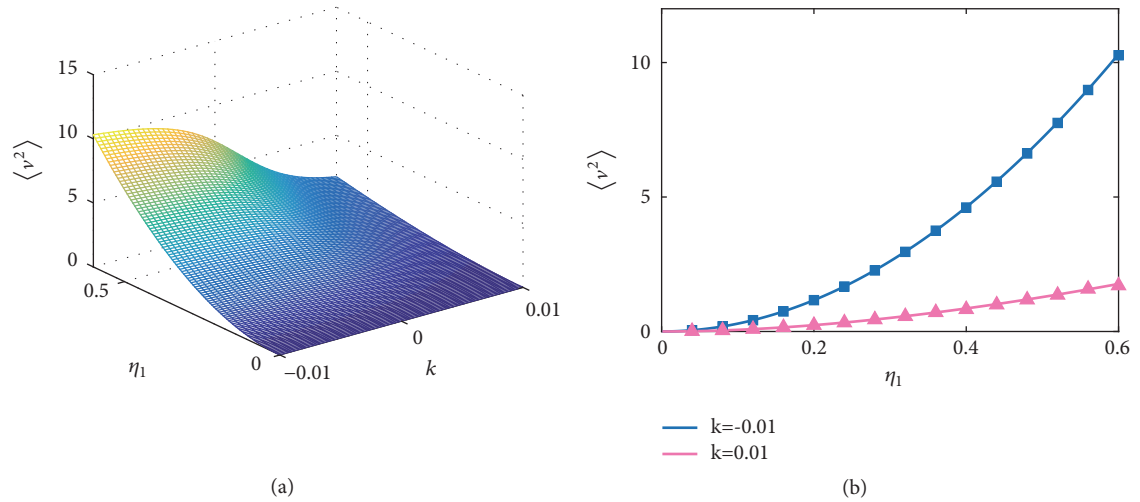

FIGURE 13: The dependence of the mean square electric voltage $\langle v^2 \rangle$ on k and η_1. Solid lines are the analytical results; symbols result from numerical simulations.

For larger η_0, the two curves almost coincide in the vicinity of the horizontal axis, implying very little mean square voltage. The observations suggest that the smaller η_0 and the bigger of the absolute value of the negative feedback help the energy harvesting system produce higher mean square voltage.

4.5. Effect of Electrical Coefficient. The dependence of the mean square electric voltage $\langle v^2 \rangle$ on η_1 and feedback strength k is depicted in Figure 13; the parameters are $\eta_0 = 0.01$, $\tau = 1.0$, $\gamma = 0.2$, $D = 0.01$. As shown in Figure 13(b), for smaller values of η_1, the two curves corresponding to $k = -0.01, 0.01$ are somewhat coincident. As η_1 increases, the two curves will gradually separate and the distance will be further and further, which reveals that the negative feedback strength induces a larger mean square voltage, approximately 5.8 times the positive feedback for $\eta_1 = 0.6$. In addition, these phenomena indicate that a larger η_1 helps to get a higher mean square electric voltage.

5. Conclusion and Discussions

In the multiple attractors wind-induced vibration energy harvester system, the birhythmic properties of the oscillator can be efficiently controlled by a time-delayed feedback. How the time-delayed feedback modify the bifurcation scenario in a general way is examined in detail, such that one may realize in the bifurcation diagram a dividing line that separates the space into two subspaces for which the dynamical scenarios are generically distinct. Depending on the time delay and its feedback strength, different regions may exist in the bifurcation diagram. The time delay feedback may play an

important role in adjusting the position of the dividing line(s) between the regions.

For the region *II* in the bifurcation diagram, the outer stable cycle is hardly affected by the time delay, which facilitates the energy harvester to collect more energy. So in the analysis of random responses, we focus on the region *I* and seek optimal control parameters. The effects of noise level, time delay and feedback intensity, time constant ratio, and coupling coefficients on the mean square voltage are systematically analyzed. All the results show that negative feedback strength can effectively improve the collection performance of the energy harvester. And when other parameters are unchanged, an optimal time delay value can be sought to maximize the system's mean square voltage. Gaussian white noise with higher noise intensity and larger coupling coefficient in the electrical equation, smaller time constant ratio, and smaller coupling coefficient in the mechanical equation can also enable the energy harvesting system to collect more energy. These findings may deepen our general understanding of the underlying mechanism of the multiple attractors wind-induced vibration energy harvester and provide a possible recipe to design energy harvesting systems with super performances in practical applications.

Appendix

The stochastic system (2), (3) can be rewritten as

$$\begin{aligned}\dot{x} &= y,\\ \dot{y} &= \mu\left(y - \frac{1}{3}y^3 + \frac{\alpha}{5}y^5 - \frac{\beta}{7}y^7\right) - w_0^2 x + \eta_0 v\\ &\quad + k\left(y_\tau - y\right) + \xi,\\ \dot{v} &= -\gamma v - \eta_1 y,\end{aligned} \tag{A.1}$$

where y_τ stands for the delayed variable $y(t-\tau)$ and ξ is Gaussian white noise. The second-order Runge–Kutta algorithm can be applied

$$\begin{aligned}x(t+h) &= x(t) + \frac{h}{2} * [F1 + F2],\\ y(t+h) &= y(t) + \frac{h}{2} * [H1 + H2],\\ v(t+h) &= v(t) + \frac{h}{2} * [K1 + K2].\end{aligned}$$

$$\begin{aligned}F1 &= y(t),\\ H1 &= \mu\left[y(t) - \frac{1}{3}y(t)^3 + \frac{\alpha}{5}y(t)^5 - \frac{\beta}{7}y(t)^7\right]\\ &\quad - w_0^2 x(t) + K\left(y(t-\tau) - y(t)\right) + R,\\ K1 &= -\gamma v(t) - \eta_1 y(t).\end{aligned}$$

$$\begin{aligned}\overline{x} &= x(t) + h * F1,\\ \overline{y} &= y(t) + h * H1,\\ \overline{v} &= \xi(t) + h * K1.\end{aligned}$$

$$\begin{aligned}F2 &= \overline{y},\\ H2 &= \mu\left[\overline{y} - \frac{1}{3}\overline{y}^3 + \frac{\alpha}{5}\overline{y}^5 - \frac{\beta}{7}\overline{y}^7\right] - w_0^2\overline{x}\\ &\quad + K\left(\overline{y}(t-\tau) - \overline{y}\right) + R,\\ K2 &= -\gamma\overline{v} - \eta_1\overline{y}.\end{aligned} \tag{A.2}$$

where $R = \sqrt{2D/h}w$ and w is a Gaussian random number.

Data Availability

No data were used to support this study.

Conflicts of Interest

The authors declare that they have no conflicts of interest.

Acknowledgments

This work was supported by the National Natural Science Foundation of China [Grants nos. 11532011, 11472212, 11772254, and 11672232] and the NPU Foundation for Fundamental Research.

References

[1] J. B. Ekanayake, L. Holdsworth, X. G. Wu, and N. Jenkins, "Dynamic modeling of doubly fed induction generator wind turbines," *IEEE Transactions on Power Systems*, vol. 18, no. 2, pp. 803–809, 2003.

[2] C. A. Kitio Kwuimy and C. Nataraj, "Recurrence and joint recurrence analysis of multiple attractors energy harvesting system," in *Structural nonlinear dynamics and diagnosis*, vol. 168 of *Springer Proc. Phys.*, pp. 97–123, Springer, Cham, 2015.

[3] L. Tang and Y. Yang, "Analysis of synchronized charge extraction for piezoelectric energy harvesting," *Smart Materials and Structures*, vol. 20, no. 8, Article ID 085022, 2011.

[4] S. Roundy and P. K. Wright, "A piezoelectric vibration based generator for wireless electronics," *Smart Materials and Structures*, vol. 13, no. 5, pp. 1131–1142, 2004.

[5] N. E. DuToit, B. L. Wardle, and S.-G. Kim, "Design considerations for MEMS-scale piezoelectric mechanical vibration energy harvesters," in *Proceedings of the Symposium on Ferroelectricity and Piezoelectricity, IMRC 2004*, pp. 121–160, Mexico, August 2004.

[6] A. Erturk and D. J. Inman, "A distributed parameter electromechanical model for cantilevered piezoelectric energy harvesters," *Journal of Vibration and Acoustics*, vol. 130, Article ID 041002, pp. 1–15, 2008.

[7] X. Jin, Y. Wang, M. Xu, and Z. Huang, "Semi-analytical solution of random response for nonlinear vibration energy harvesters," *Journal of Sound and Vibration*, vol. 340, pp. 267–282, 2015.

[8] S. Zhou and L. Zuo, "Nonlinear dynamic analysis of asymmetric tristable energy harvesters for enhanced energy harvesting," *Communications in Nonlinear Science and Numerical Simulation*, vol. 61, pp. 271–284, 2018.

[9] T. L. Djomo Mbong, M. Siewe Siewe, and C. Tchawoua, "Controllable parametric excitation effect on linear and nonlinear vibrational resonances in the dynamics of a buckled beam," *Communications in Nonlinear Science and Numerical Simulation*, vol. 54, pp. 377–388, 2018.

[10] D. Mallick, A. Amann, and S. Roy, "Surfing the High Energy Output Branch of Nonlinear Energy Harvesters," *Physical Review Letters*, vol. 117, no. 19, 2016.

[11] S. Zhou, J. Cao, D. J. Inman, S. Liu, W. Wang, and J. Lin, "Impact-induced high-energy orbits of nonlinear energy harvesters," *Applied Physics Letters*, vol. 106, no. 9, p. 093901, 2015.

[12] L.-Q. Chen, W.-A. Jiang, M. Panyam, and M. F. Daqaq, "A broadband internally resonant vibratory energy harvester," *Journal of Vibration and Acoustics*, vol. 138, no. 6, 2016.

[13] G. Sebald, H. Kuwano, D. Guyomar, and B. Ducharne, "Experimental Duffing oscillator for broadband piezoelectric energy harvesting," *Smart Materials and Structures*, vol. 20, no. 10, 2011.

[14] N. Tran, M. H. Ghayesh, and M. Arjomandi, "Ambient vibration energy harvesters: a review on nonlinear techniques for performance enhancement," *International Journal of Engineering Science*, vol. 127, pp. 162–185, 2018.

[15] Z. Xu, X. Shan, D. Chen, and T. Xie, "A novel tunable multi-frequency hybrid vibration energy harvester using piezoelectric and electromagnetic conversion mechanisms," *Applied Sciences*, vol. 6, no. 1, 2016.

[16] Z. Yang, Y. Zhu, and J. Zu, "Theoretical and experimental investigation of a nonlinear compressive-mode energy harvester with high power output under weak excitations," *Smart Materials and Structures*, vol. 24, no. 2, 2015.

[17] M. F. Daqaq, "On intentional introduction of stiffness nonlinearities for energy harvesting under white Gaussian excitations," *Nonlinear Dynamics*, vol. 69, no. 3, pp. 1063–1079, 2012.

[18] E. Halvorsen, "Erratum: Fundamental issues in nonlinear wideband-vibration energy harvesting (Physical Review E - Statistical, Nonlinear, and Soft Matter Physics (2013) 87 (042129))," *Physical Review E: Statistical, Nonlinear, and Soft Matter Physics*, vol. 88, no. 3, 2013.

[19] F. Cottone, H. Vocca, and L. Gammaitoni, "Nonlinear energy harvesting," *Physical Review Letters*, vol. 102, no. 8, Article ID 080601, 2009.

[20] M. F. Daqaq, "Transduction of a bistable inductive generator driven by white and exponentially correlated Gaussian noise," *Journal of Sound and Vibration*, vol. 330, no. 11, pp. 2554–2564, 2011.

[21] A. Erturk and D. J. Inman, "Broadband piezoelectric power generation on high-energy orbits of the bistable Duffing oscillator with electromechanical coupling," *Journal of Sound and Vibration*, vol. 330, no. 10, pp. 2339–2353, 2011.

[22] L. Haitao, Q. Weiyang, L. Chunbo, D. Wangzheng, and Z. Zhiyong, "Dynamics and coherence resonance of tri-stable energy harvesting system," *Smart Materials and Structures*, vol. 25, no. 1, 2015.

[23] G. T. Oumbé Tékam, C. A. Kitio Kwuimy, and P. Woafo, "Analysis of tristable energy harvesting system having fractional order viscoelastic material," *Chaos: An Interdisciplinary Journal of Nonlinear Science*, vol. 25, no. 1, 013112, 10 pages, 2015.

[24] L. Haitao, Q. Weiyang, L. Chunbo, D. Wangzheng, and Z. Zhiyong, "Dynamics and coherence resonance of tri-stable energy harvesting system," *Smart Materials and Structures*, vol. 25, no. 1, 2016.

[25] H. Farokhi and M. H. Ghayesh, "Nonlinear mechanics of electrically actuated microplates," *International Journal of Engineering Science*, vol. 123, pp. 197–213, 2018.

[26] H. Farokhi and M. H. Ghayesh, "Supercritical nonlinear parametric dynamics of Timoshenko microbeams," *Communications in Nonlinear Science and Numerical Simulation*, vol. 59, pp. 592–605, 2018.

[27] M. H. Ghayesh, H. Farokhi, and A. Gholipour, "Oscillations of functionally graded microbeams," *International Journal of Engineering Science*, vol. 110, pp. 35–53, 2017.

[28] T. Yildirim, M. H. Ghayesh, W. Li, and G. Alici, "Design and development of a parametrically excited nonlinear energy harvester," *Energy Conversion and Management*, vol. 126, pp. 247–255, 2016.

[29] T. Yildirim, M. H. Ghayesh, W. Li, and G. Alici, "A nonlinearly broadband tuneable energy harvester," *Journal of Dynamic Systems, Measurement, and Control*, vol. 139, no. 1, 2017.

[30] K. Makihara, Y. Yamamoto, K. Yoshimizu, C. Horiguchi, H. Sakaguchi, and K. Fujimoto, "A novel controller to increase harvested energy from negating vibration-suppression effect," *Smart Materials and Structures*, vol. 24, no. 3, 2015.

[31] N. E. Karakasis and C. A. Mademlis, "High efficiency control strategy in a wind energy conversion system with doubly fed induction generator," *Journal of Renewable Energy*, vol. 125, pp. 974–984, 2018.

[32] Z. Sun, J. Fu, Y. Xiao, and W. Xu, "Delay-induced stochastic bifurcations in a bistable system under white noise," *Chaos: An Interdisciplinary Journal of Nonlinear Science*, vol. 25, no. 8, 083102, 6 pages, 2015.

[33] Z. K. Sun, W. Xu, X. L. Yang, and T. Fang, "Inducing or suppressing chaos in a double-well Duffing oscillator by time delay feedback," *Chaos, Solitons & Fractals*, vol. 27, no. 3, pp. 705–714, 2006.

[34] V. Semenov, A. Feoktistov, T. Vadivasova, E. SchÖll, and A. Zakharova, "Time-delayed feedback control of coherence resonance near subcritical Hopf bifurcation: theory versus experiment," *Chaos: An Interdisciplinary Journal of Nonlinear Science*, vol. 25, no. 3, 033111, 6 pages, 2015.

[35] P. Ghosh, S. Sen, S. S. Riaz, and D. S. Ray, "Controlling birhythmicity in a self-sustained oscillator by time-delayed feedback," *Physical Review E: Statistical, Nonlinear, and Soft Matter Physics*, vol. 83, no. 3, Article ID 036205, 9 pages, 2011.

[36] Q. Guo, Z. Sun, and W. Xu, "Stochastic bifurcations in a birhythmic biological model with time-delayed feedbacks," *International Journal of Bifurcation and Chaos*, vol. 28, no. 4, 1850048, 14 pages, 2018.

[37] D. Biswas, T. Banerjee, and J. Kurths, "Control of birhythmicity: a self-feedback approach," *Chaos: An Interdisciplinary Journal of Nonlinear Science*, vol. 27, no. 6, 063110, 11 pages, 2017.

[38] K. Pyragas, "Continuous control of chaos by self-controlling feedback," *Physics Letters A*, vol. 170, no. 6, pp. 421–428, 1992.

[39] W. Q. Zhu and Z. H. Liu, "Response of quasi-integrable Hamiltonian systems with delayed feedback bang-bang control," *Nonlinear Dynamics*, vol. 49, no. 1-2, pp. 31–47, 2007.

[40] W.-A. Jiang and L.-Q. Chen, "Stochastic averaging of energy harvesting systems," *International Journal of Non-Linear Mechanics*, vol. 85, pp. 174–187, 2016.

[41] Z. H. Liu and W. Q. Zhu, "Stochastic averaging of quasi-integrable Hamiltonian systems with delayed feedback control," *Journal of Sound and Vibration*, vol. 299, no. 1-2, pp. 178–195, 2007.